SUPPLEMENTARY MATERIAL

SAMPLE AND SITE DESCRIPTIONS

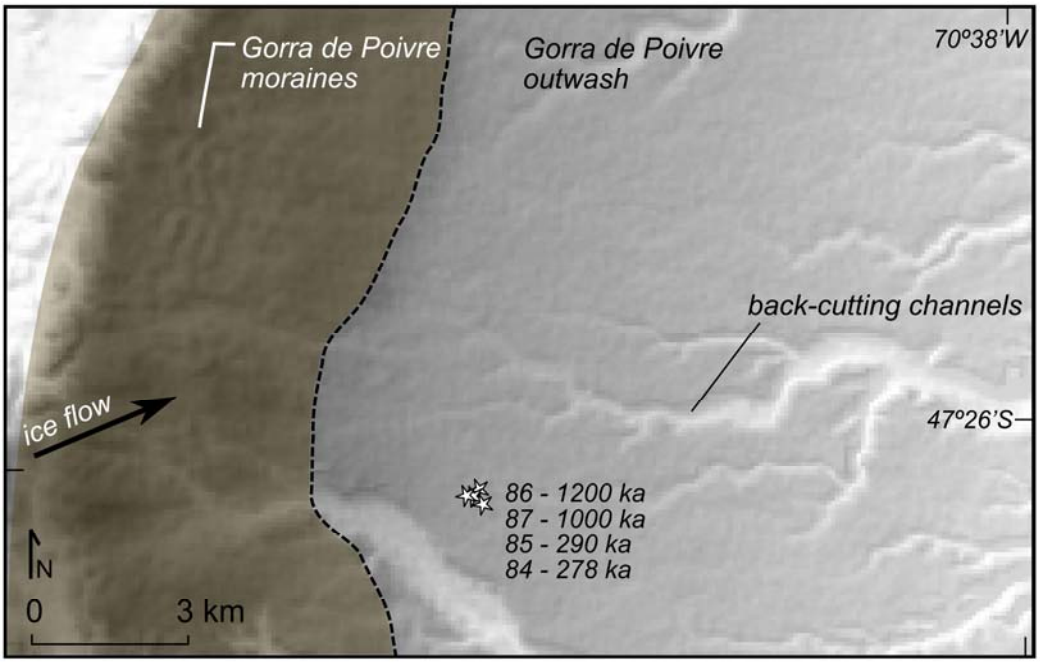

Figure DR1 shows the context of the sample location on the Gorra de Poivre outwash terrace illustrated in Figure 1 of the main document (shaded SRTM 90m DEM). The dark shading covers till associated with the Gorra de Poivre moraines, these grade eastward into the Gorra de Poivre outwash terrace, which was sampled a few kilometers from the ice limit (dashed). From the DEM, it is possible to see that the samples (stars - labelled with sample ID and ^{10}Be exposure ages) were taken from a flat and stable location on the terrace surface, at the interfluve between erosive drainage channels that incise into the outwash gravels.

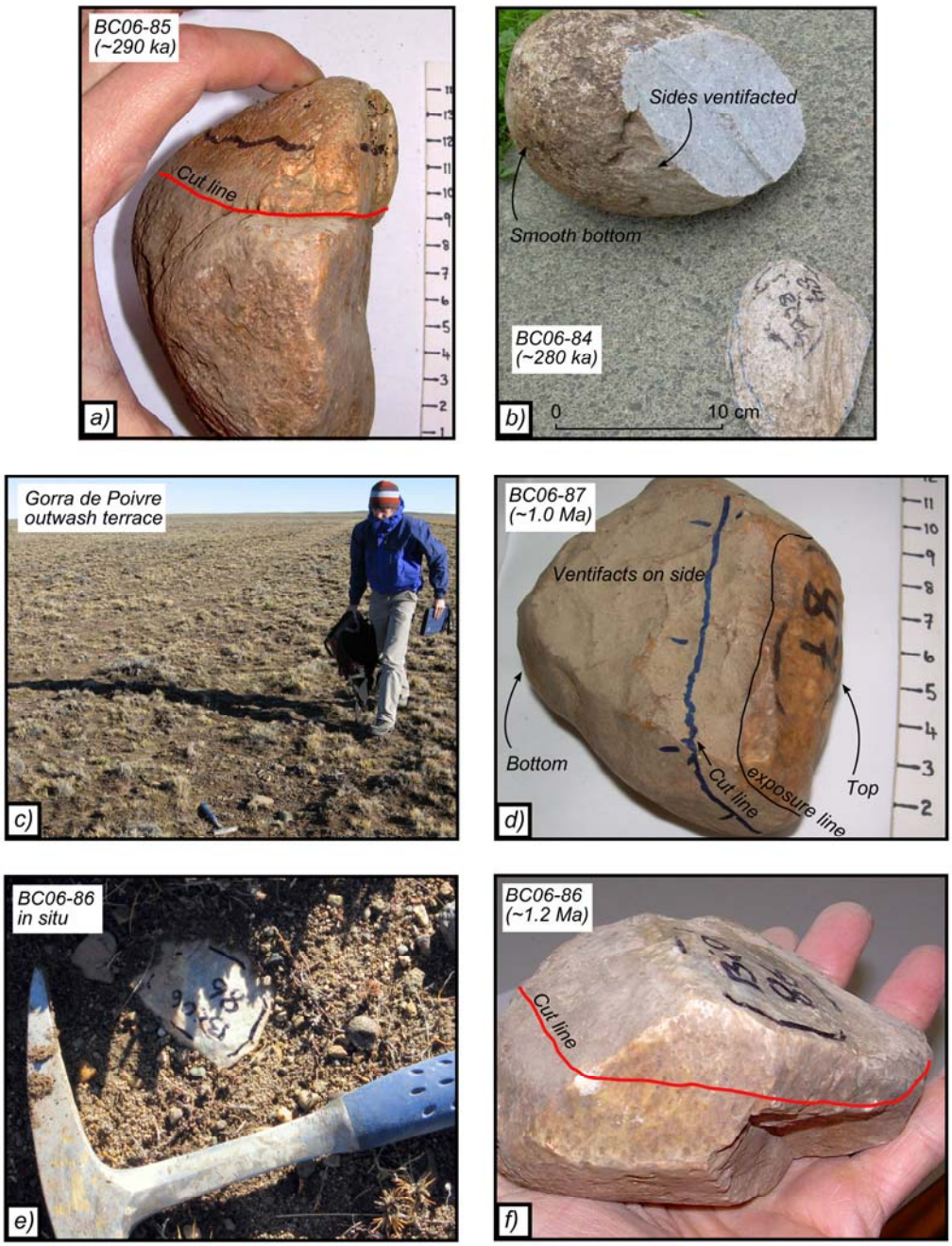

Figure DR2 shows the samples that were taken from the surface, their ages, and a view of the terrace surface itself (Fig. DR2c). It is evident the oldest cobbles are more severely eroded than the youngest, which still had a clear fluvial form and no ventifacts on their bottom surfaces. The location of where the sample was cut is indicated.

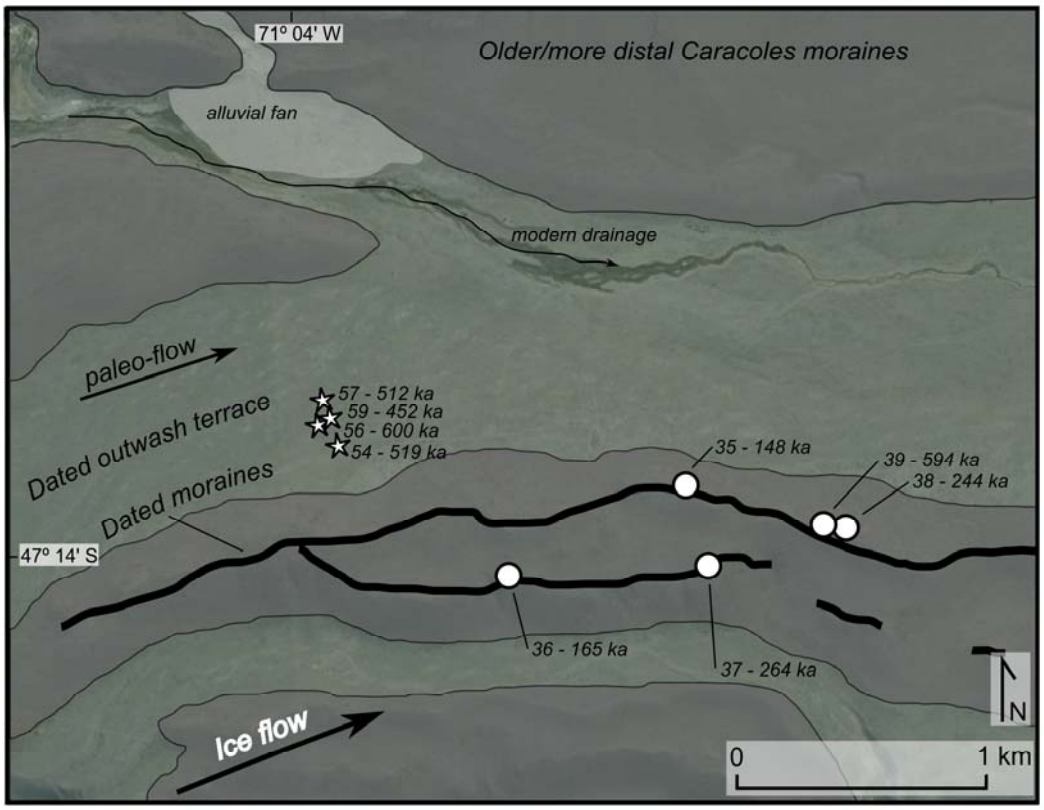

Figure DR3 shows the context of the sample locations in the Cañadon de Caracoles system illustrated in Figure 1 of the main document. The Google Earth image is overlaid by dark shading over moraine material and light green shading over outwash material. The dated moraine limit (black solid lines) grades into the dated outwash terrace surface to its north. Moraine boulder (circles) and outwash cobble (stars) sample locations and ^{10}Be ages are shown. The outwash cobbles were sampled from a location on the terrace where it appeared stable and where there was no evidence of mixing of older sediment from the terraces and moraines behind (to the north of) the outwash terrace.

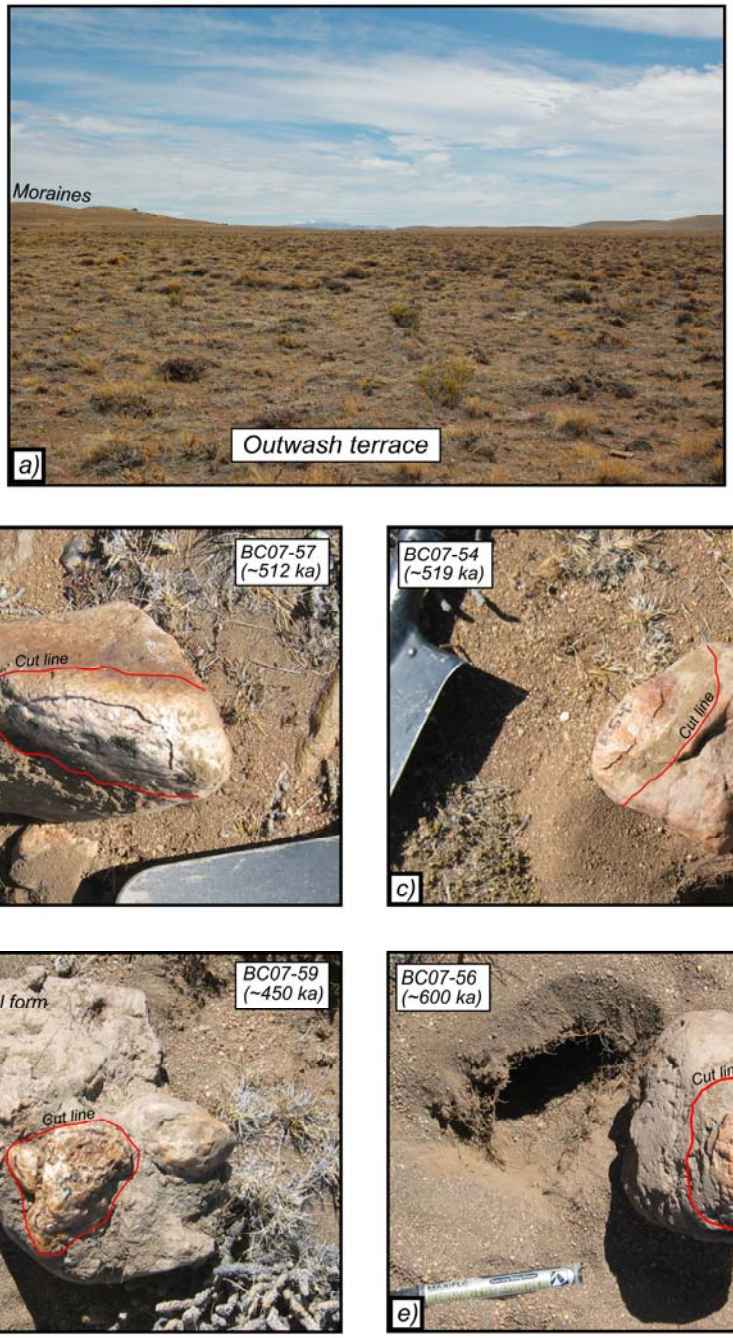

Photos of the samples, their ages, and where they were cut are shown in Figure DR4. All cobbles had ventifacts on their exposed surfaces; however sample BC07-59 was severely eroded (Fig. DR4d) obliterating the inferred former glaciofluvial shape of the top surface. It is possible the nodule sampled from this cobble was not as close to the original surface as was thought.

The moraines were sampled where they appear best preserved. Boulder samples were collected with hammer and chisel from two moraines. Boulders from the outermost moraine yield both the oldest and the youngest ages.

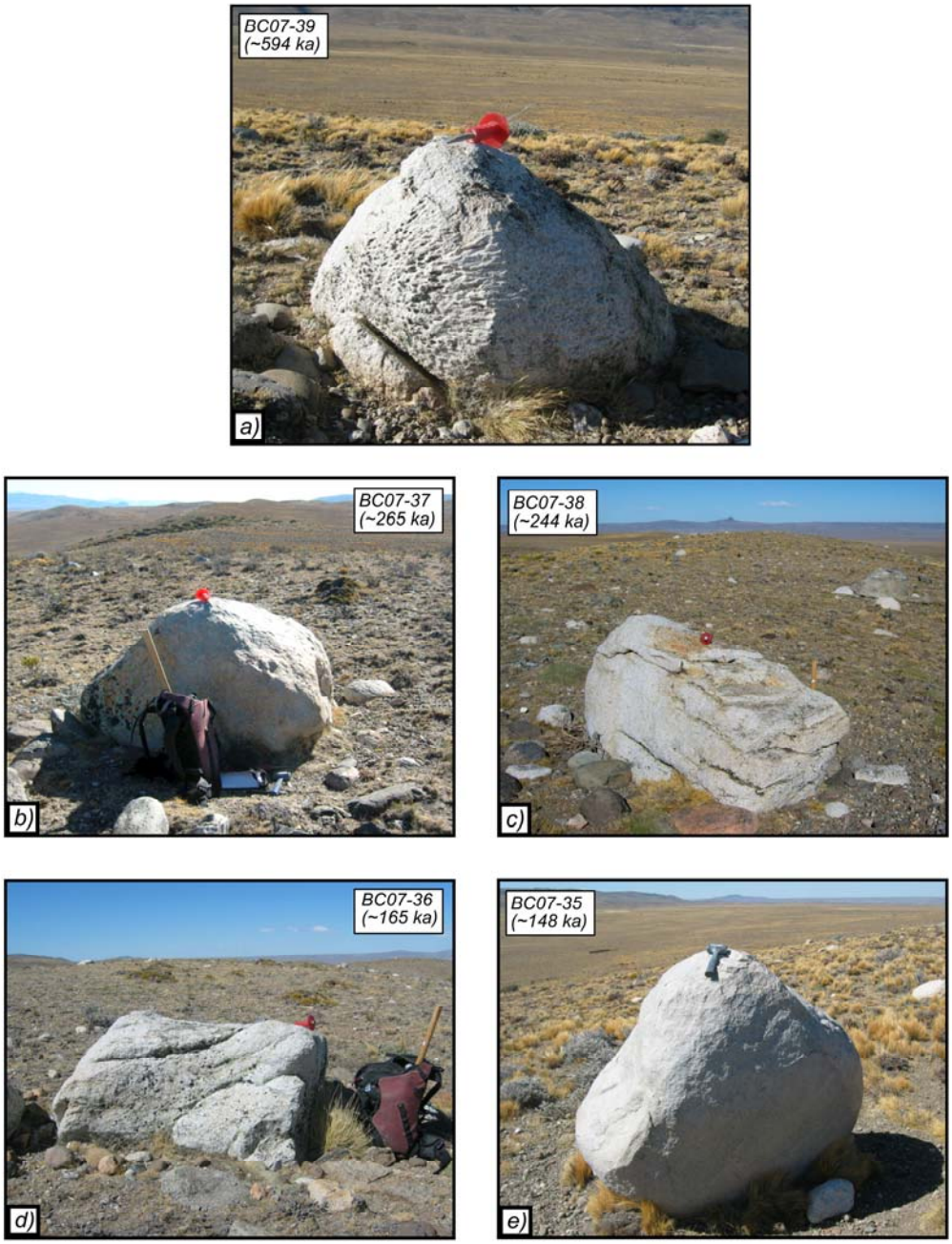

Photographs of the sampled boulders and their ages are shown in Figure DR5. The oldest boulder (BC07-39) is homogenously and severely ventifacted below 50cm (Fig. DR5a). Note that the younger boulders show comparatively less aeolian erosion, indicating a comparatively recent exposure at the surface (as compared to the oldest boulder).

Sample coordinates and further sample specific information are provided in Table DR1.

SAMPLE PREPARATION AND ANALYSIS

The samples were prepared at the University of Edinburgh's Cosmogenic Isotope Laboratory following an adaptation of the methods of Kohl and Nishiizumi (1992) and Bierman et al. (2002) (Hein, 2009). Samples were cut (if required) to an appropriate thickness (1 – 4 cm) and were then crushed and sieved to obtain the 250 – 710 μm fraction which was used for analysis. The AMS measurements were performed at the Scottish Universities Environmental Research Centre (S.U.E.R.C.). ^{10}Be concentrations are normalized to the NIST SRM-4325 Be standard material with a revised nominal ^{10}Be/^{9}Be ratio of 2.79 x 10^{-11} (Nishiizumi et al., 2007). ^{26}Al concentrations are normalized to the Purdue Z92-0222 Al standard material with a nominal ^{26}Al/^{27}Al ratio of 4.11 x 10^{-11} which agrees with the Al standard material of Nishiizumi et al. (2004). The corresponding ^{26}Al/^{10}Be production rate ratio is 6.75.

The analytical results are presented in Table DR2. Nuclide concentrations in Table DR2 are corrected for the number of ^{10}Be and ^{26}Al atoms in their associated blanks. Blanks (n = 5) were spiked with 250 μg ^{9}Be carrier (Scharlau 1000 mg/l; density 1.02; Batch# 81145) and 1.5 mg ^{27}Al carrier (Fischer 1000 ppm; Batch# 0736322). Samples were spiked with 250 μg ^{9}Be carrier and up to 1.5 mg ^{27}Al carrier (the latter value varied depending on the native Al-content of the sample). For each batch of 7 samples one blank was processed. The corresponding combined process and carrier blanks range between 115,000 ± 18,000 atoms ^{10}Be and 290,000 ± 40,000 atoms ^{10}Be (< 1% of total ^{10}Be atoms in sample; 0.9 – 1.7 x 10^{-14} [^{10}Be/^{9}Be]); and between 61,000 ± 12,000 atoms ^{26}Al and 190,000 ± 57,000 atoms ^{26}Al (< 1% of total ^{26}Al atoms in sample; 2.6 – 3.8 x 10^{-15} [^{26}Al/^{27}Al]). Sample and blank ^{10}Be/^{9}Be and ^{26}Al/^{27}Al analytical uncertainties and a 2% carrier addition uncertainty and 3% stable ^{27}Al measurement (ICP-OES) uncertainty are propagated into the 1σ analytical uncertainty for nuclide concentrations.

Exposure ages were calculated with the CRONUS-Earth web-based calculator (version 2.2 ;Balco et al., 2008)[1] which implements the revised ^{10}Be standardization and half-life (1.36 Ma) of Nishiizumi et al. (2007). Sample thickness (Table DR1) and density (2.7 g cm^{3} assumed) are used to correct for self-shielding. Topographic shielding was measured with an inclinometer (horizons < 3º) but corrections are considered negligible for all samples (scaling factor < 0.9998). Present day winter snow cover is thin and short-lived and models predict increased aridity during glacial times (Hulton et al., 2002). Therefore, because the semi-arid conditions are thought to have persisted through time, no correction is applied for snow cover or for shielding by vegetation. No erosion rate correction is applied because the fluvial form of the cobbles suggests that total rock surface erosion is generally negligible. However, for boulders, ages corrected for an erosion rate of 1.4 mm ka^{-1} are provided alongside the uncorrected ages; the erosion rate value was derived by Kaplan et al. (2005) for boulders on the Telken moraines at Lago Buenos Aires, 60 kilometers to the north. Uncorrected (for erosion) boulder-ages are used throughout the paper. The exposure ages are reported based on the Dunai (2001) scaling model. Exposure ages differ by <6% depending on the scaling model used.

[1] (http://hess.ess.washington.edu/math/index_dev.html)

ADDITIONAL DISCUSSIONS

Production rate increase

The time-averaged ^{10}Be and ^{26}Al production rates near Lago Pueyrredón have been estimated to be 5% and 11% higher than for standard atmospheric conditions by two independent studies that infer a low pressure anomaly during glacial times (see Ackert et al., 2003; Hein et al., 2009; Staiger et al., 2007). Following Staiger et al.(2007), we increase the ^{10}Be and ^{26}Al production rates by 5%. Importantly, the choice of production rates does not affect our main conclusions. The higher production rate is implemented within the exposure age calculator by artificially lowering the air pressure at the sampled locations, thereby increasing the production rate (Hein et al., 2009). Specifically, we lower the sea-level pressure that is used in the conversion of sample elevations to sample air pressures; the present day sea-level pressure (1009.3 hPa)[2] is lowered to 1002.3 hPa. The lower sea-level pressure reduces the calculated sample air pressures, and thereby increases the time-averaged production rate derived through the calculator by approximately 5% when compared against the value obtained from a calculation based on the present day sea-level pressure.

Exhumation of cobbles

We estimate that on the Gorra de Poivre outwash terrace, the youngest outwash cobble age (BC06-84) probably reflects exhumation from a minimum depth of 75 cm. This is a rough approximation assuming the terrace has not inflated or deflated, and is ~1.2 Ma as the oldest cobble indicates, and assuming a soil density of 2.2 g cm^{-3}. To obtain the estimate, we modelled the nuclide concentration with depth using Equation 6 in Granger and Smith (2000). The time-averaged ^{10}Be production rate at the sample location (10.01 atoms ^{10}Be g^{-1} a^{-1}) was derived using the CRONUS-Earth exposure age calculator (cf., Hein et al., 2009). The minimum depth is ~90 cm, but this reduces to ~75 cm if we consider self-shielding with the sample oriented upside down during transit to the surface (either by erosion or up-freezing).

Oldest boulder age on Caracoles Moraine

The oldest moraine boulder (BC07-39) gives an exposure age that is indistinguishable from the oldest outwash cobble age. This exposure age would increase significantly with even low erosion rates. The boulder's top surface appeared as an original glaciofluvial shape, but the lower 50 cm had large ventifacts on its windward side (Fig. DR5a). The intensity of ventifaction is homogenous in the affected area, making a gradual exhumation of the boulder unlikely. Sand and dust particles are not normally lifted above ca. 50 cm (Bagnold, 1941), thus it is possible the boulder remained on the moraine crest but the top surface escaped significant aeolian erosion by virtue of its height. Alternatively, if erosion would be deemed significant, the high age could indicate the moraine deposit is significantly older than 600 ± 20 ka (age inferred from cobbles), or that the boulder contains inherited nuclides. The rather tight clustering of cobble ages renders the former unlikely, and the latter would require that the boulder is a solitary occurrence of significant pre-exposure in over 60 ^{10}Be measurements in the valley (Hein *et al.*, 2010; 2009). Overall, aeolian erosion

[2] NCEP-NCAR reanalysis; www.cdc.noaa.gov/ncep_reanalysis/

rates may have been relatively low at this location on the northern margin of the valley.

Aeolian erosion

The principal mechanism for rock surface erosion is by aeolian processes (i.e., sand-blasting). Geologic observations indicate that aeolian erosion is episodic given the presence of rock varnish on ventifacts (Fig. 3b; Hein et al., 2009). It also appears to have been more intense towards the center of the valley where rock surfaces are severely ventifacted on comparatively young surfaces. The active outwash terraces are the primary source of erosive windblown dust as shown more widely in Patagonia (Sugden et al., 2009), and these terraces are most extensive in the center of the valley where wind speeds are generally higher (e.g., Chock and Cochran, 2005). It may be that rocks on the northern margin of the valley (e.g., on the Cañadon de Caracoles moraines) are relatively protected from sand blasting because there is a lack of major dust sources upwind, assuming the prevailing wind direction has been from the west. Thus, we speculate that overall, erosion rates may have been lower at these locations.

REFERENCES CITED

Ackert, R. P., Singer, B. S., Guillou, H., Kaplan, M. R., and Kurz, M. D. (2003). Long-term cosmogenic He-3 production rates from Ar-40/Ar-39 and K-Ar dated Patagonian lava flows at 47 degrees S. *Earth and Planetary Science Letters* **210,** 119-136.

Balco, G., Stone, J. O., Lifton, N. A., and Dunai, T. J. (2008). A complete and easily accessible means of calculating surface exposure ages or erosion rates from Be-10 and Al-26 measurements. *Quaternary Geochronology* **3,** 174-195.

Bierman, P. R., Caffee, M. W., Davis, P. T., Marsella, K., Pavich, M., Colgan, P., Mickelson, D., and Larsen, J. (2002). Rates and timing of earth surface processes from in situ-produced cosmogenic Be-10. *In* "Beryllium: Mineralogy, Petrology, And Geochemistry." pp. 147-205. Reviews In Mineralogy & Geochemistry. Mineralogical Soc America, Washington.

Chock, G. Y. K., and Cochran, L. (2005). Modeling of topographic wind speed effects in Hawaii. *Journal of Wind Engineering and Industrial Aerodynamics* **93,** 623-638.

Dunai, T. J. (2001). Influence of secular variation of the geomagnetic field on production rates of in situ produced cosmogenic nuclides. *Earth and Planetary Science Letters* **193,** 197-212.

Hein, A. S. (2009). "Quaternary Glaciations in the Lago Pueyrredón Valley, Argentina." Unpublished PhD thesis, University of Edinburgh.

Hein, A. S., Hulton, N. R. J., Dunai, T. J., Schnabel, C., Kaplan, M. R., and Xu, S. (2009). Middle Pleistocene glaciation in Patagonia dated by cosmogenic nuclide measurements on outwash gravels. *Earth and Planetary Science Letters***,** doi:10.1016/j.epsl.2009.06.026.

Hulton, N. R. J., Purves, R. S., McCulloch, R. D., Sugden, D. E., and Bentley, M. J. (2002). The Last Glacial Maximum and deglaciation in southern South America. *Quaternary Science Reviews* **21,** 233-241.

Kaplan, M. R., Douglass, D. C., Singer, B. S., and Caffee, M. W. (2005). Cosmogenic nuclide chronology of pre-last glacial maximum moraines at Lago Buenos Aires, 46 degrees S, Argentina. *Quaternary Research* **63,** 301-315.

Kohl, C. P., and Nishiizumi, K. (1992). Chemical Isolation of Quartz for Measurement of Insitu-Produced Cosmogenic Nuclides. *Geochimica et Cosmochimica Acta* **56,** 3583-3587.

Nishiizumi, K. (2004). Preparation of Al-26 AMS standards. *Nuclear Instruments & Methods in Physics Research Section B* **223-24,** 388-392.

Nishiizumi, K., Imamura, M., Caffee, M. W., Southon, J. R., Finkel, R. C., and McAninch, J. (2007). Absolute calibration of Be-10 AMS standards. *Nuclear Instruments & Methods in Physics Research Section B* **258,** 403-413.

Staiger, J., Gosse, J., Toracinta, R., Oglesby, B., Fastook, J., and Johnson, J. V. (2007). Atmospheric scaling of cosmogenic nuclide production: Climate effect. *Journal of Geophysical Research-Solid Earth* **112**.

Sugden, D. E., McCulloch, R. D., Bory, A. J. M., and Hein, A. S. (2009). Influence of Patagonian glaciers on Antarctic dust deposition during the last glacial period. *Nature Geoscience* **2,** 281-285.

TABLE DR1. SAMPLE DESCRIPTIONS

ID	Latitude (dd)	Longitude (dd)	Altitude (m asl)	Type*-lithology	Size† (cm)	Thickness (cm)	Comments
Gorra de Poivre							
BC06-86	-47.44816	-70.77132	813	OWC-quartz	12	2	ventifacts on all sides
BC06-87	-47.44814	-70.77102	814	OWC-quartz	10	2	ventifacts on all sides
BC06-85	-47.44815	-70.77153	811	OWC-volcanic	14	3	ventifacts only on top/sides
BC06-84	-47.44801	-70.77122	811	OWC-volcanic	19	3	ventifacts only on top/sides
Cañadon de Caracoles							
BC07-56	-47.22905	-71.06558	765	OWC-quartz	17	2.5	ventifacts on top surface only
BC07-54	-47.23013	-71.06517	765	OWC-quartz	18	2.5	ventifacts on top surface only
BC07-57	-47.22843	-71.06575	760	OWC-quartz	26	3	ventifacts on top surface only
BC07-59	-47.22927	-71.06602	765	OWC-quartz	27	2	ventifacts on top only - significant erosion
BC07-39	-47.23422	-71.03812	769	MB-granite	**60**x115x100	2.5	severe ventifacts on west side below 50 cm
BC07-37	-47.23533	-71.04555	762	MB-granite	**95**x160x135	1	ventifacts on west side, exfoliating (1-2 cm)
BC07-38	-47.2339	-71.03913	775	MB-granite	**100**x100x200	1.5	ventifacts on surface, horizontal fractures
BC07-36	-47.23498	-71.05643	766	MB-granite	**75**x130x130	1.5	wide boulder, horizontal fractures
BC07-35	-47.23227	-71.04653	775	MB-granite	**130**x90x160	3	Narrow base, fresh appearance

*OWC-outwash cobble, MB-moraine boulder.

† Refers to long axis for cobbles; dimension of boulders with height listed first (bold).

TABLE DR2. COSMOGENIC-NUCLIDE DATA

ID	Quartz mass (g)	Isotope AMS ID*	Nuclide concentration† (10^6 atom g^{-1})	$^{26}Al/^{10}Be$	Age 1§ (10^3 a) ε = 0		Age 2 (10^3 a) ε = 1.4 mm ka^{-1}#	
					± 1σ (int)	± 1σ (ext)	± 1σ (int)	± 1σ (ext)
Gorra de Poivre								
BC06-86	2.8949	^{10}Be – b2949	8.898 ± 0.202	5.06 ± 0.30	1211 ± 36	200		
		^{26}Al – a870	45.019 ± 2.501		1103 ± 100	260		
BC06-87	16.3597	^{10}Be – b2950	7.710 ± 0.172	5.21 ± 0.30	999.0 ± 28	160		
		^{26}Al – a871	40.192 ± 2.108		909.3 ± 71	190		
BC06-85	1.4703	^{10}Be – b2948	2.637 ± 0.086	6.63 ± 0.48	290.3 ± 9.8	38		
		^{26}Al – a867	17.488 ± 1.136		305.1 ± 22	48		
BC06-84	17.3231	^{10}Be – b2947	2.534 ± 0.056	6.03 ± 0.34	278.0 ± 6.4	36		
		^{26}Al – a866	15.284 ± 0.788		261.4 ± 15	38		
Cañadon de Caracoles								
BC07-56	20.7016	^{10}Be – b1773	4.862 ± 1.46	5.71 ± 0.36	599.6 ± 20	85		
		^{26}Al – a645	27.76 ± 1.52		566.9 ± 39	98		
BC07-54	18.9782	^{10}Be – b2044	4.283 ± 1.14	6.01 ± 0.37	518.9 ± 15	72		
		^{26}Al – a650	25.75 ± 1.41		514.3 ± 35	87		
BC07-57	19.9434	^{10}Be – b1774	4.199 ± 1.30	--	512.0 ± 17	71		
	--	--	--	--	--			
BC07-59	18.3588	^{10}Be – b2045	3.813 ± 1.01	5.96 ± 0.36	452.4 ± 13	61		
		^{26}Al – a651	22.73 ± 1.24		435.9 ± 28	70		
BC07-39	20.1155	^{10}Be – b2086	4.844 ± 1.44	5.48 ± 0.34	594.4 ± 20	84	Saturated	
		^{26}Al – a667	26.54 ± 1.45		531.9 ± 36	90	Saturated	
BC07-37	15.0548	^{10}Be – b2054	2.353 ± 0.073	5.83 ± 0.37	264.3 ± 8.5	34	422.4 ± 23	100
		^{26}Al – a656	13.71 ± 0.751		237.9 ± 14	35	361.5 ± 35	91
BC07-38	21.44	^{10}Be – b2085	2.198 ± 0.067	6.71 ± 0.42	243.9 ± 7.7	32	368.1 ± 18	79
		^{26}Al – a664	14.74 ± 0.810		256.5 ± 15	38	412.6 ± 44	120
BC07-36	20.2027	^{10}Be – b2084	1.504 ± 0.046	6.45 ± 0.41	165.0 ± 5.1	21	209.2 ± 8.4	35
		^{26}Al – a663	9.701 ± 0.532		162.7 ± 9.3	23	206.7 ± 15	39
BC07-35	17.8902	^{10}Be – b2083	1.347 ± 0.038	6.47 ± 0.41	147.7 ± 4.2	19	181.9 ± 6.5	29
		^{26}Al – a662	8.713 ± 0.493		145.5 ± 8.5	20	179.4 ± 13	32

*AMS measurements made at Scottish Universities Environmental Research Centre (SUERC).

†Normalised to NIST SRM-4325 Be standard material with a revised (Nishiizumi et al., 2007) nominal $^{10}Be/^{9}Be$ ratio (2.79×10^{-11}) and half-life (1.36 Ma), and the Purdue Z92-0222 Al standard material with a nominal $^{27}Al/^{26}Al$ ratio of 4.11×10^{-11} that agrees with Al standard material of Nishiizumi et al. (2004). Nuclide concentrations include propagated AMS sample/lab-blank uncertainty, 2% carrier mass uncertainty (Be) and 3% stable ^{27}Al measurement (ICP-OES) uncertainty.

§Ages calculated with CRONUS-Earth exposure age calculator version 2.2 (Balco et al., 2008) and Dunai (2001) scaling factor. The production rate was increased by 5% (see text). (int) = analytical uncertainties; (ext) = propagated external uncertainties.

#Erosion rate from Kaplan et al.(2005).